Nuclear Physics A402 (1983) 87–113

SPIN DETERMINATION VIA α-d ANGULAR CORRELATIONS AND α-TRANSFER DWBA ANALYSIS IN ^{18}F HIGH-ENERGY STATES

M. C. ETCHEGOYEN†, D. SINCLAIR, A. ETCHEGOYEN† and E. BELMONT MORENO††

Nuclear Physics Laboratory, Oxford OX1 3RH, England

Received 19 November 1982
(Revised 14 January 1983)

Abstract: Particle particle angular correlations for reactions in non-zero degree geometry and with non-zero spin nuclei were investigated and found to be a valuable tool for spin determination. d-α angular correlations for ^{14}N(^{6}Li, d)^{18}F* → (α)^{14}N were measured for three strongly excited states in ^{18}F (9.58 MeV, 11.2 MeV and 14.1 MeV), at 36 MeV of bombarding energy. Spins and parities for two of the observed states were determined, and, in agreement with theoretical predictions, these states are suggested as members of the $K^\pi = 1^+$ α-rotational band. The three analyzed states are found to undergo a predominant α-particle decay to the ground state of ^{14}N. Angular distributions for all the observed states are measured and analyzed under Hauser-Feshbach and exact-finite-range DWBA formalisms with Gamow unbound wave functions. Spectroscopic factors are extracted and compared to the shell-model predictions showing a reasonable agreement.

E NUCLEAR REACTIONS ^{14}N(^{6}Li, d), E = 36 MeV; measured $\sigma(\theta d)$, $\alpha d(\theta)$. ^{18}F resonances deduced J, π, α-branching, S_x. Optical model, Hauser-Feshbach, exact finite-range DWBA analyses, cluster model interpretation.

1. Introduction

Several investigations on four-particle cluster structure have been performed lately. Alpha-transfer reactions as (^{6}Li, d) and (^{7}Li, t) have shown [1–4]) a high selectivity in the final state population of light nuclei. With the experimental evidence of substantial four-particle clustering in sd-shell nuclei, many rotational bands with a $J(J+1)$ dependence have been identified and different models have been suggested to describe these cluster states. They range from the shell model to simpler cluster models as the folded potential model introduced by Buck, Dover and Vary (BDV) [5]). However, the connection between model states and experimental levels is in many cases hindered by the lack of definite spin-parity assignments.

Some α-transfer experiments on ^{14}N, performed with ^{13}C(105 MeV) and ^{11}B(115 MeV) incident beams [6]) had shown strong population of ^{18}F states between 9 and

† Present address: Comisión Nacional de Energía Atómica, Buenos Aires, Argentina.
†† On leave of absence from Inst. Nac. de Investigaciones Nucleares, México.

16 MeV of excitation energy. No detailed study of these states was possible due to the lack of spin assignments and further investigation on α-transfer on ^{14}N was suggested. Exploratory runs with ^{6}Li incident ions were performed at a bombarding energy of 36 MeV. They showed deuteron spectra of striking selectivity closely following the pattern found by Cobern and Parker[1]) in the ^{14}N(^{7}Li, t)^{18}F reaction. Some of the low-lying levels observed here were seen by Rolfs *et al.*[7]) in their work on ^{14}N(α, γ), and identified as members of a $K^{\pi} = 1^{+}$ 4p-2h rotational band. States of strong population are formed at 9.58, 11.2 and 14.1 MeV of excitation energy. The first two states were already observed by Cobern and Parker who suggested that they might be higher members of the above mentioned band. This in turn suggested that the selectively populated states, also found in the (^{6}Li, d) reaction, were mainly 4p–2h states. A cluster model[8]) was suggested which predicted the existence of such a band and the excitation energies of some of its members. Tests could be performed on the ability of the cluster, shell and rotational models in predicting experimental results, if the higher spin states of this band were identified. The high counting rate observed for the peaks of interest, the fact that these states are unbound to α-decay and the knowledge that transfer reactions induced by heavy ions do not normally have angular distribution shapes strongly dependent on the spin of the final state, suggest the particle-particle (d-α) angular correlation as a plausible method for spin determination. Nonzero-degree geometry angular correlations have been extensively used with (^{6}Li, d) and (^{7}Li, t) reactions[9–12]) for spin assignments since the experimental techniques are greatly simplified when detecting away from the beam direction. Even more, the study of the displacement of the symmetry axis for the sequential decay from the second direction provides in some cases[13]) the necessary information to select the reaction mechanism involved. The α-decay of the highly populated states in the recoil nucleus (^{18}F) is observed, aiming at spin and parity assignments. Angular distributions for the primary reactions are studied as well, for completeness to the suggested assignments.

2. Experimental details

Angular distributions and angular correlation experiments were performed at the Oxford Nuclear Physics Laboratory with a ^{6}Li ion beam of 36 MeV and typical currents of 200–400 nA from the Folded Tandem accelerator. The target, natural ^{14}N (99.6 % purity) was contained in a cylindrical gas cell with an internal diameter of 6 cm and at typical pressures of 100–150 Torr. Rectangular apertures of 1.2 cm × 1.3 cm for the entrance window and 1.2 cm × 7.2 cm for a wide exit window were sealed with thin 5 μm aluminium foils. Typical gas cell collimation systems of three tantalum collimators for each detector were used.

For the elastic scattering, a $\Delta E - E$ semiconductor detector assembly with a 73.2 μm ΔE component and a 2.2 mm E-detector was positioned at 25 cm from the

target centre, and the laboratory angle varied from 8° to 35° from the beam direction. The angular distribution for the stripping reaction was obtained with a different $\Delta E - E$ assembly (ΔE component of 200 μm and E-component of 4.1 mm) in order to supress elastically scattered ^{6}Li ions from being recorded in coincidence with α-signals. The detector system was positioned at 8°, 9°, 11°, 12°, 14°, 16°, 18°, 20°, 23° and 26° from the beam axis in the laboratory frame. The ΔE and E pulses were amplified and directly sent to fast Silena analog to digital converters (ADCs). The logic signals obtained from pulses above noise level were sent to a coincidence box and the output signals obtained when this requirement was fulfilled gated the ADCs in a delayed coincidence mode. The dead time corrections were carried out with the use of a precision pulser triggered externally by the output signal of the Faraday cup current digitizer. The ΔE and E signals were processed on- and off-line for particle identification with the use of a PDP11/60 computer system. A typical deuteron spectrum taken at 16° is shown in fig. 1. Overall energy resolution of approximately 250 keV was obtained.

For the angular correlation measurements, the detection of ejectiles coming from the initial transfer reaction was performed with the same "telescope" $\Delta E - E$ detector assembly used for the angular distribution experiments. This was situated at 16° from the beam direction in the laboratory frame. Decay particles from the recoil nucleus were detected with five single silicon surface barrier detectors ranging from 1500 to 2000 μm. These detectors were spaced 15° from each other and on the opposite side of the chamber (with respect to the beam direction) to the

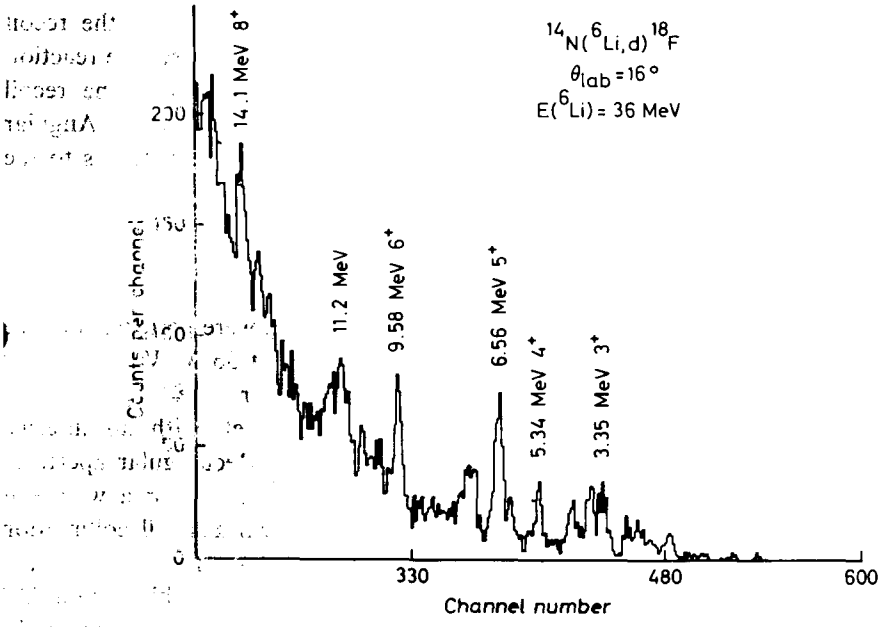

Fig. 1. Deuteron energy spectrum for the ^{14}N(^{6}Li, d)^{18}F reaction at 36 MeV and θ_{lab} = 16°.

"telescope". The collimation system for the decay particle detection was arranged in order to look at the same active region of the gas cell as that of the "telescope" collimation system, thus collimation distances were carefully selected. The electronic circuit employed was a standard particle-particle coincidence assembly.

Fast Silena ADCs were used for the ΔE and E signals gated in prompt mode. A box named "interrupt encoder", developed in this laboratory was used for processing the singles and coincidence signals. It has eight input sockets each one with a different priority according to its place. When more than one input pulse reaches the encoder, only the one with higher priority is processed. If single events are not required, the corresponding inputs can be disabled, thus reducing the dead time and securing that only coincidence events are written onto magnetic tape. This CAMAC box transfers to the PDP11/60 computer the information on the particular detector (route) which generated the signal. As single counters were used for the residual nucleus decay detection, the corresponding particle identification was obtained from the kinematics. ^{18}F states with excitation energies above 4.4159 MeV, 5.606 MeV and 7.526 MeV are unstable against α,- p- and d-emission, respectively. For that reason, their kinematics were also studied in order to identify different particles in the decay spectra and select the angular position of the detectors avoiding kinematical crossings of α-particles with protons or deuterons.

3. The ^{14}N(^{6}Li, d)^{18}F transfer reaction and ^{18}F $\rightarrow$ ^{14}N + α decay

In order to obtain a good theoretical prediction for the particle-particle angular correlation, it is necessary to know the reaction mechanism involved in the transfer process to the residual state and the decay process to the daughter nucleus, and to have a good model for the transfer and decay matrices needed in the theoretical expression for the angular correlation (appendix A). For this reason, angular distributions were measured and theoretically calculated for the spins of interest within the framework of direct and Hauser-Feshbach formalisms. The results obtained for the already known members of the $K^{\pi} = 1^{+}$ band (1.7 MeV (1^{+}), 2.52 MeV (2^{+}), 3.35 MeV (3^{+}), 5.35 MeV (4^{+}) and 6.56 MeV (5^{+})), as well as for the unknown spin states (9.58 MeV, 11.2 MeV and 14.1 MeV) showed a compound nucleus contribution of less than 10 % for all cases (sect. 4). The attention was focused then to the direct process (some assessments about the possibility of multistep contributions will be discussed in sect. 6) and transition amplitudes from DWBA codes were used in the estimation of theoretical angular correlations. All possible relevant values of spin and parity were studied for the three high-lying states. For some spin assumptions, the theoretical predictions were structureless, while for some others, a very strong oscillatory behaviour characteristic of the spin of the recoil nucleus was found. For many of these oscillatory cases, the strong structure vanished as the angle of the detected ejectile increased.

All states in ^{18}F above 4.4159 MeV are α-unbound. It has been shown [14]) that simplified prescriptions for describing those unbound states are not satisfactory in DWBA calculations; hence the wave functions for the ^{18}F levels have been represented by Gamow states. Within this formalism, the unbound states are treated as spectroscopically equivalent to bound states.

The possible orbital angular momenta of the α-cluster with respect to the core are given by the triangular rule $\boldsymbol{L}_\alpha = \boldsymbol{I}' + \boldsymbol{I}''$, where $\boldsymbol{I}'$ stands for the initial spin of the decaying nucleus and $\boldsymbol{I}''$ is the spin of the daughter nucleus formed in the α-decay. When parities of parent and final states are the same, only even values of L_α are allowed, while in the case of opposite parities odd values of L_α are allowed. The experimental decay spectra showed that the peaks of strong population were those corresponding to α-decay of the ^{18}F states to the ground state of the ^{14}N daughter nucleus ($J^\pi = 1^+$, $T = 0$). The first noticeable difficulty for the α-decay analysis is that for several final spin values, two possible orbital angular momenta are allowed, and therefore, the spectroscopic coefficients and the decay matrices (A_{lsj} and $S^{I'}_{s'',L_\alpha}$ of eq. (A.7)) have to be known in order to perform the theoretical calculation. When parentage amplitudes were available from shell-model calculations, these were used in obtaining the spectroscopic coefficients. For the rest, a study of the variation of the resultant angular correlation for different relative values of the spectroscopic factors was performed. At the same time, the influence of using different decay $S^{I'}_{s'',L_\alpha}$ matrices in the theoretical angular correlation expression was investigated for

$$|S^{I'}_{s'',L_{\alpha 1}}|^2 + |S^{I'}_{s'',L_{\alpha 2}}|^2 = 1, \tag{2}$$

and phases determined by $e^{i\phi}$ with $\phi = 0$, $\frac{1}{2}\pi$, π and $\frac{3}{2}\pi$ (appendix B). The theoretical angular correlations obtained for the different sets of values A_{lsj} and $S^{I'}_{s'',L_\alpha}$ were compared to the experimental ones with a χ^2 test in order to find the best fit. Fig. 2 shows a typical analysis for fixed spectroscopic amplitudes and different combinations of the decay $S^{I'}_{s'',L_\alpha}$ matrices with an assumed $J^\pi = 8^-$ for the 14.1 MeV state in ^{18}F. For all states with two L_α contributions, the minimum values resultant from these systematic analyses were used in the final chi-square comparison for spin assignment. When spin and parity assumptions allowed only one L_α contribution, the analysis was simpler since only one A_{lsj} and $S^{I'}_{s'',L_\alpha}$ value intervenes in the theoretical expression for the angular correlation, and both can be taken as constant multiplicative factors which will not affect the angular correlation shape.

4. Hauser-Feshbach calculations

The reaction ^{14}N(^{6}Li, d)^{18}F at bombarding energies high above the Coulomb barrier ($E_{\text{Coul}} = 5.11$ MeV) is expected to be predominantly direct. Even so,

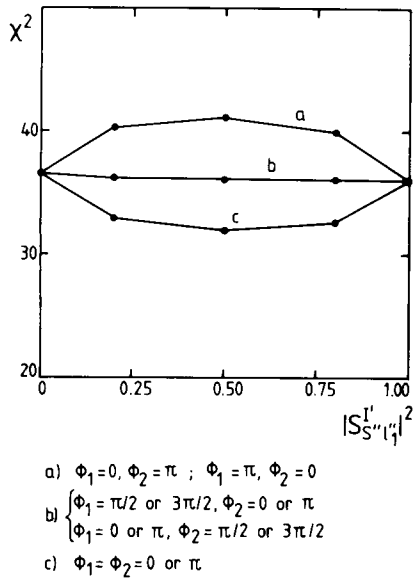

Fig. 2. χ^2 comparison between the experimental angular correlation for the 14.1 MeV state in ^{16}F and the theoretical estimation for a supposed 8^-. Different combinations of $S^{l'}_{s''l''}$ values have been considered. The solid lines join points for which a similar phase convention has been adopted.

reaction mechanism studies of (^{6}Li, d) reactions on neighbouring nuclei have shown for some cases [i.e. ^{12}C(^{6}Li, d)^{16}O at 20 MeV of ^{6}Li, ref. [4])] an important contribution of the compound nucleus mode. House *et al.* [15]) in their work on ^{16}O(^{6}Li, d)^{20}Ne found small compound nuclear contributions at 20, 24 and 28 MeV of bombarding energies. Hauser-Feshbach calculations have been performed with the code STATIS [16]) in order to estimate the importance of the compound nucleus mechanism in our reaction. The dependence of the magnitude of Hauser Feshbach calculations on the choice of the critical angular momentum for the compound nucleus formation has been widely studied in the literature [17,18]). The computer code STATIS allows the fixing of the critical angular momentum by an external setting of a lower bound for the entrance channel transmission coefficients (T_l) in the calculation. No need for either sharp or soft cut off model approximations are required as the transmission coefficients are obtained directly from optical model results. Several calculations were performed with different lower bounds and no appreciable variations in the cross sections were found for critical angular momenta (l_c) larger than 11. This value was used for the calculations presented in this work. Six open channels including the elastic scattering, protons, neutrons, deuterons, α-particles and ^{3}He channels were considered, closely following refs. [3,16,19]). The optical parameters used are reported in table 1. The comparison with experimental results is shown in figs. 3a and 3b. For the three

TABLE 1

Level density and optical model parameters used in HF calculations

Channel	^{6}Li+^{14}N	n+^{19}Ne	p+^{19}F	d+^{18}F	^{3}He+^{17}O	α+^{16}O
δ(MeV^{-1})	3.3	3.3	3.3	3.3	3.3	3.3
Δ(MeV)	0.0	2.25	2.25	0.0	2.25	4.5
number of discrete levels	12	19	14	12	20	15
V(MeV)	195.45 [a]	48.45	50.6	94.3 [a]	146.1	125.0
R_V (fm)	3.3	3.2	2.855	2.69	3.54	4.96
a_V (fm)	0.653	0.71	0.74	0.806	0.638	0.50
W (MeV)	14.09 [a]	7.06 [b]	7.10 [b]	7.49 [a]	22.08 [b]	5.0 [b]
R_W (fm)	4.67	3.2	3.41	5.7	3.499	4.96
a_W (fm)	0.878	1.0	0.7	0.56	0.636	0.50
R_c (fm)	3.3	3.34	3.2	3.47	3.214	3.527
$V_{s.o.}$ (MeV)		5.0	8.0			
$R_{Vs.o.}$ (fm)		3.2	2.908			
$a_{Vs.o.}$ (fm)		0.71	0.74			
reference	this work	[34]	[35]	[36]	[37]	[38]

δ and Δ are the level density and pairing parameters, respectively. The radii follow the definition: $R = r_0(A^{\frac{1}{3}} + A_T^{\frac{1}{3}})$.

[a]) Woods-Saxon. [b]) Woods-Saxon derivate W.

highest energy levels analysed, several compound nucleus estimations are observed, since these calculations were done for different possible spin values of these three states. As can be clearly seen, even the largest estimations for the compound nuclear mechanism are small when compared with the experimental cross sections.

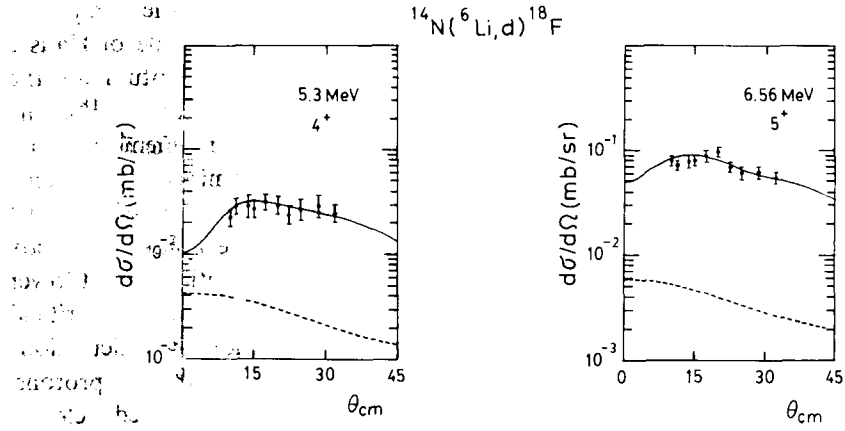

Fig. 5a. Angular distributions of deuterons from the ^{14}N(^{6}Li, d)^{18}F reaction at $E(^6\text{Li}) = 36$ MeV leading to the 5.3 MeV 4$^+$ and 6.56 MeV 5$^+$. The dotted lines show Hauser-Feshbach calculations. The solid curves are normalised DWBA predictions.

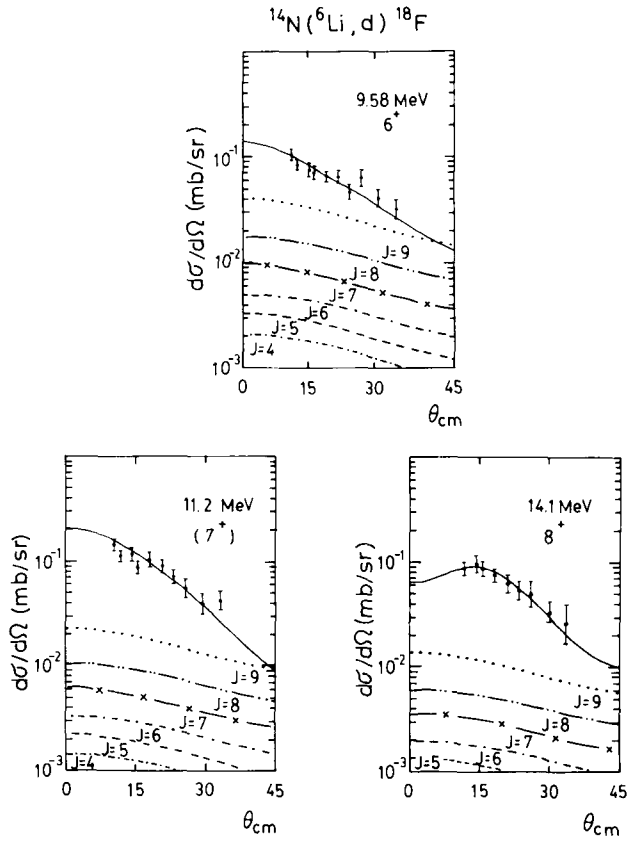

Fig. 3b. Angular distributions of deuterons from the ^{14}N(^{6}Li, d)^{18}F reaction at $E(^{6}\text{Li}) = 36$ MeV leading to the 9.58 MeV, 11.2 MeV and 14.1 MeV states. The dotted lines show Hauser-Feshbach calculations for different spin assumptions. The solid curves are normalised DWBA predictions.

It is well known that the magnitude of the cross section depends strongly on the level density parameter. All compound nucleus calculations shown here were carried out with level density parameters obtained from the literature for (^{6}Li, d) reactions. Changes to a typical level density parameter suggested by Stokstad [16] for the sd-shell ($a = 2.88$ MeV^{-1}) gave variations up to 30 % which would nevertheless produce a small contribution to the present studies. The process is then, analysed under the direct transfer reaction mode with the use of exact-finite-range DWBA calculations and recoil effects included.

5. Angular correlation results

For the three high excited states in ^{18}F, the coincidence spectra showed a very strong α-emission leading to the ground state of ^{14}N. A typical decay spectrum at

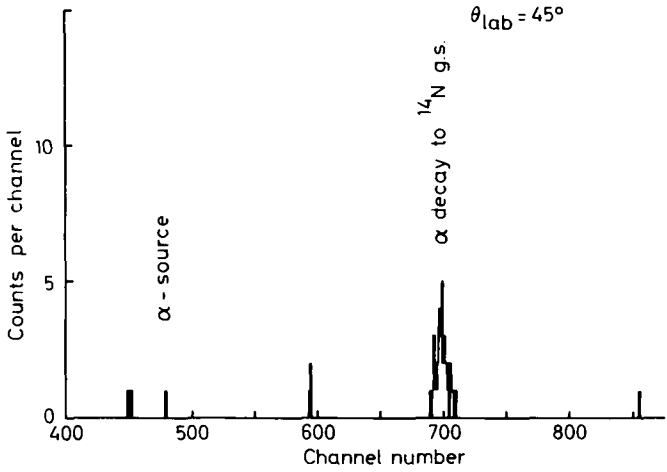

Fig. 4. Decay spectrum for the 11.2 MeV state in ^{18}F.

45° laboratory angle recorded in coincidence with the state at 11.2 MeV in ^{18}F is shown in fig. 4. Gamow functions were obtained to represent the unbound states for each spin examined, and coupled to a DBWA code to describe the transfer reaction. The calculated reduced amplitudes were then used as input for an angular correlation computing code.

5.1. THE 9.58 MeV STATE IN ^{18}F

Spectra for particle decay from this state were obtained in on- and off-line analyses with a coincidence requirement between the 9.58 MeV excited state in the deuteron spectrum and the five side counters. The number of α-d coincidences for this state was the lowest of the three levels analysed in ^{18}F. Even so, the correlation observed showed a clear and smooth undulatory behaviour as can be seen in fig. 5. The errors pictured in the experimental angular correlation are the statistical errors. The theoretical results were compared to the experimental values obtained (fig. 5) and a chi-square test was performed. These latter results are depicted in fig. 6 and show a clear preference for a 6^+ spin and parity assignment. This is strongly reinforced by the χ^2 test that gives for the 6^+ assignment a probability of at least a factor of 7 larger than for the other spins. In fig. 5 different fits to the experimental 9.58 MeV angular correlation for even spins in the $2N+L=8$ band are exhibited.

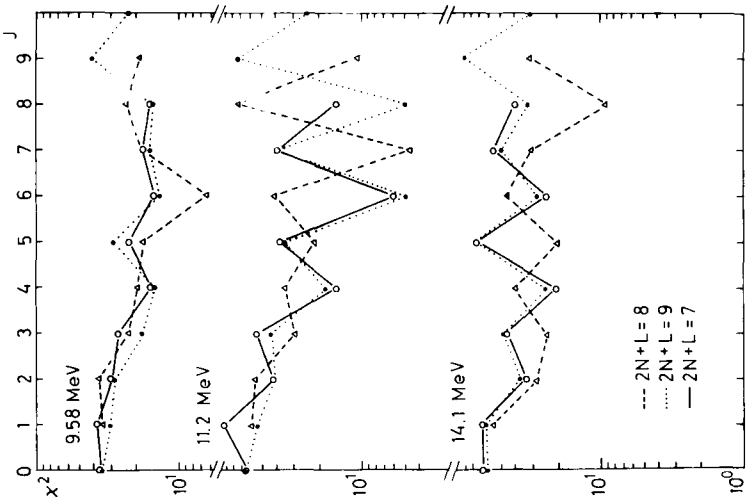

Fig. 6. χ^2 values obtained in fitting different theoretical predictions to the α-d angular correlation data for the 9.58 MeV 11.2 MeV and 14.1 MeV states. The lines are for guiding the eye in identifying each particular 2N+L value.

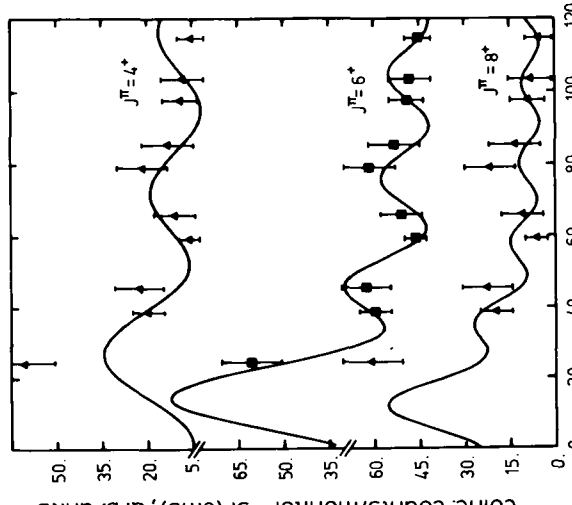

Fig. 5. α-d angular correlation for the 9.58 MeV state. The three different fits are applied to the same data.

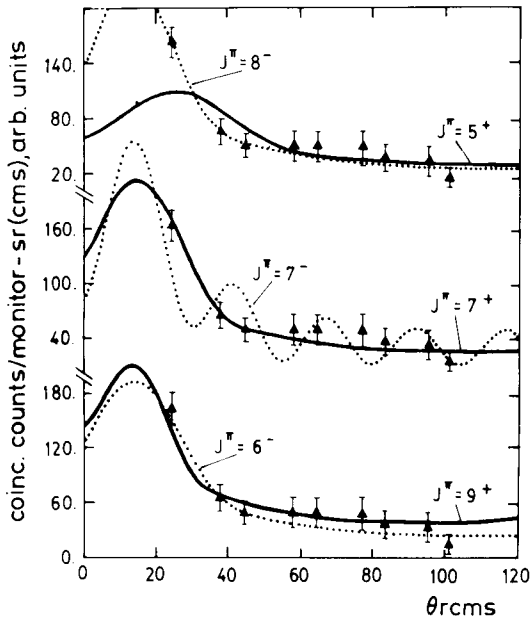

Fig. 7. α-d angular correlation for the 11.2 MeV state in ^{18}F. The six different fits are applied to the same data.

5.2. THE 11.2 MeV STATE IN ^{18}F

The number of α-d coincidences registered for this state was higher than those observed for the 9.58 MeV state by a factor of 2. The experimental angular correlation for the alpha emission shows a typical structureless pattern found for the states in which mixing of two L-values takes place (fig. 7), and several theoretical correlation functions can be regarded as good fits to the experimental data for different allowed spin values. The results for these comparisons are shown in fig. 6. The best chi-square values are obtained alternatively for odd spins with positive parities and even spins with negative parities in a range of angular momenta between 6 and 9. For the $2N+L = 8$ band, the χ^2 comparison shows a favored 7^+ over the 9^+ assignment, while $2N+L = 7$ and 9 bands give almost indistinct preference to 6^- and 8^- spins. In spite of the suggestive $2N+L = 8$ band structure which may be theoretically expected for α-transfer reactions on ^{14}N, no spin assignments can be made due to the lack of characteristic angular momentum shape.

5.3. THE 14.1 MeV STATE IN ^{18}F

The number of α-d coincidences for this state was larger than those observed for

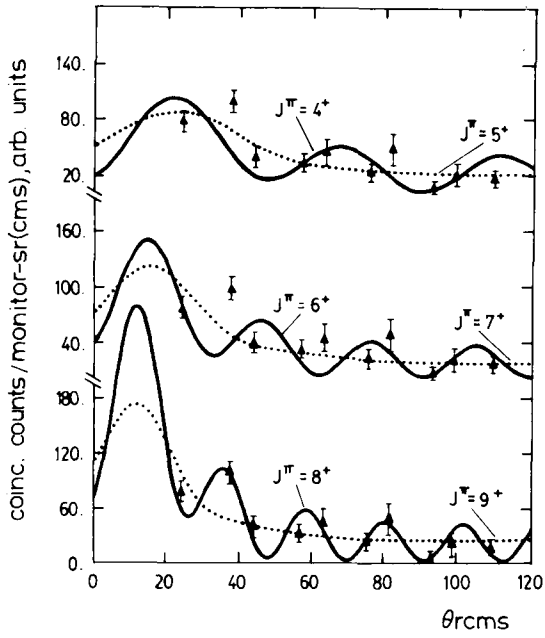

Fig. 8. α-d angular correlation for the 14.1 MeV state in ^{18}F. The six different fits are applied to the same data.

the 9.58 MeV state by a factor of 3. Since the 14.1 MeV state appears on a high part of the continuous deuteron background, a larger random contribution was expected for this level than for the previously mentioned one. Careful studies of coincidences with neighbouring zones to the peak of interest were performed in order to estimate their contribution to the different spectra. The experimental angular correlation obtained is pictured in fig. 8. It shows a strongly undulatory behaviour which matches preferably the theoretical correlation for the $J^\pi = 8^+$ ($2N+L = 8$). The different values obtained from χ^2 comparisons with all the spin possibilities considered ($2N+L = 7$, 8 and 9) (fig. 6) indicate clearly that the $J^\pi = 8^+$ assignment is the favoured one. The χ^2 test gives for an 8^+ assignment a probability of at least a factor of 20 larger than for the other spins.

6. ^{14}N(^{6}Li, d)^{18}F: the reaction mechanism

Quantitative analyses of the direct process contribution to the reaction dynamics have been performed by using the distorted wave Born approximation (DWBA). Zero-range and no-recoil approximations commonly used in light ion works for estimating the DWBA transition amplitude are not appropriate for the quantitative analysis of heavy ion transfer reactions. For this reason, recoil and finite-range

DWBA calculations have to be performed. Even more, all interaction potentials which are usually supposed to cancel out, should be included in the transition amplitude in order to achieve post-prior agreement [20]). An extension of the BDV model for the α-cluster unbound states in ^{18}F is used to calculate the wave functions in terms of Gamow states. For the projectile description, the work of Kubo and Hirata [21]) for the ^{6}Li = d + α was followed. The EFR-DWBA calculations were performed with Gamow unbound wave functions describing the heavy system and a modified version [6]) of the computing code LOLA.

6.1. OPTICAL POTENTIALS

Typical optical potentials for the different channels involved are required for both, the compound nucleus and the direct transfer calculations. Optical potentials for the entrance channel have been obtained by fitting the optical model predictions to the collected elastic scattering data. The elastic scattering of a 36 MeV ^{6}Li beam off a ^{14}N gas target between 8° and 35° in the laboratory system was measured. The angular distributions obtained, as well as the optical model fits are shown in fig. 9, with the corresponding parameters given in table 2. The search on the parameters was performed with the code DWAVF which uses a modified [23]) version of the distorted wave routine used in the DWBA code MARS [24]). The choice of the optical potentials for the exit channel was more complex, since: (i) the optical potential which describes the ground-state elastic scattering is not necessarily the appropriate prediction for an excited state of the residual nucleus, and (ii) no data are available for elastic scattering of deuterons off

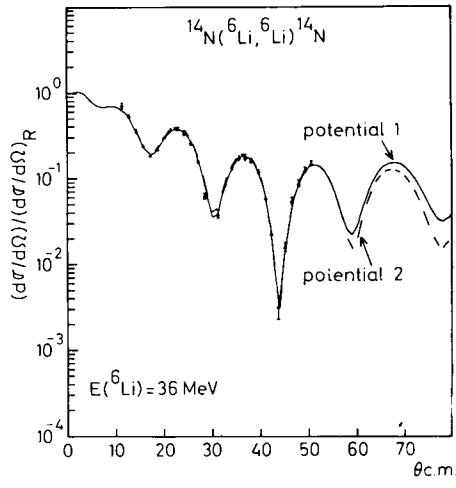

Fig. 9. Angular distribution measured for ^{6}Li elastic scattering on ^{14}N at 36 MeV bombarding energy. The theoretical curves are the optical model fits using potentials 1 and 2 of table 2.

TABLE 2

Optical potentials used in EFR-DWBA calculations

Channel	^{6}Li+^{14}N	^{6}Li+^{14}N	d+^{18}F	d+^{14}N
V_0 (MeV)	147.63	195.45	94.30	128.09
r_{0V} (fm)	0.971	0.782	1.027	1.00
a_V (fm)	0.543	0.653	0.806	0.697
W_0 (fm)	39.01	14.09	7.49	4.995
r_{0W} (fm)	0.504	1.106	2.175	1.946
a_W (fm)	1.273	0.878	0.560	0.856
r_{0c} (fm)	0.971	0.782	1.30	1.30
reference	this work	this work	[36])	this work and ref. [26])
number	1	2	3	4
inc. energy	36 MeV	36 MeV	15 MeV	11.8 MeV

The optical potentials are given by $U(r) = -V_0 f_V(r, R_V, a_V) - iW_0 f_W(r, R_W, a_W) + V_c(r)$, where $f_V(r, R_V, a_V) = \{1+\exp[(r-R_V)/a_V]\}^{-1}$, and similary for $f_W(r, R_W, a_W)$:

$$V_c(r) = \begin{cases} z_p Z_T \dfrac{e^2}{r}, & \text{for } r \geq R_c \\ z_p Z_T \dfrac{e^2}{2R_c}\left(3 - \dfrac{r^2}{R_c^2}\right), & \text{for } r < R_c, \end{cases}$$

$$R = r_0(A_p^{1/3} + A_T^{1/3}).$$

the β-unstable ^{18}F. On the other hand, a wide range of optical potentials can be obtained from the literature for elastic scattering of deuterons on neighbouring nuclei [25]). It has been shown by DeVries [20]) that in multinucleon heavy-ion transfer reactions, post-prior discrepancies indicate that all the interaction terms have to be included in the transition amplitude. Therefore in our reaction, $V_{d^{14}N} - U_{d^{18}F}$ or $V_{d^{14}N} - U_{^6Li^{14}N}$ though usually neglected should be included in the calculations. $V_{d^{14}N}$ represents the interaction between the deuteron and ^{14}N, and $U_{d^{18}F}(U_{^6Li^{14}N})$ the distorting potential for the exit (entrance) channel. According to DeVries, coulomb interactions for each of them might need to be included as well; he suggests for the latter the usual form of a uniform spherical charge, and for $V_{d^{14}N}$ an optical potential description. Potential $V_{d,^{14}N}$ was approximated by a potential that fits the elastic scattering of deuterons off ^{14}N at a bombarding energy $E(d) = E(^6Li) \times$ mass of deuteron/mass of ^{6}Li $\approx$ 12 MeV. Data were found in the literature for d+^{14}N at 11.8 MeV [ref. [26])]. These potentials included spin-orbits terms, and as in the present code at Oxford there is not such possibility, a new optical potential was searched in order to fit the same data. The results are shown in fig. 10, and the parameters given in table 2. For testing the post-prior equivalence and the influence of including all the interaction terms a bound state in ^{18}F (2^+ at 2.524 MeV) was used. The results obtained using post and prior

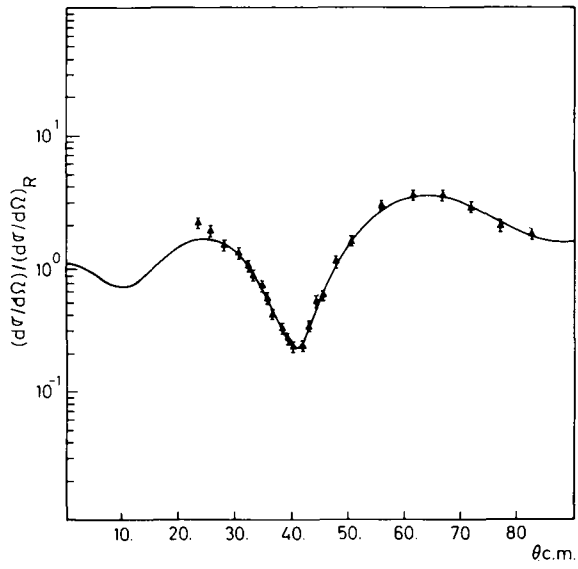

Fig. 10. Angular distribution for ^{2}H elastic scattering on ^{14}N at 11.8 MeV bombarding energy [data taken from ref. [26])]. The theoretical curve is the optical model fit using potential 5 of table 2.

forms with and without the inclusion of Coulomb terms, $V_{d^{14}N}$, $U_{^6Li^{14}N}$ and $U_{d^{18}F}$ potentials are shown in fig. 11. As expected there was a strong discrepancy in the resultant cross section for the post and prior forms with the omission of the extra interaction terms. The Coulomb potentials do not appreciably change the calculated cross sections as expected for these low charge nuclei, but when considering the two terms $V_{d^{14}N}$ and U a noticeable decrease is observed for the post form, reducing the discrepancies in the total cross sections to a 5.8 %. The total cross section for the six cases above mentioned are shown in table 3. The normalization factors for all the cross sections shown in fig. 11 were taken equal to one.

TABLE 3

Effect of extra interaction terms in the cross section

Case	$d\sigma/d\Omega$ ($\theta_{c.m.} = 20°$) (arb. units)	σ total (arb. units)
PR	0.953 E+00	0.246 E+00
PPC	0.941 E+00	0.243 E+00
PRT	0.388 E−01	0.573 E−02
PO	0.422 E−01	0.590 E−02
POC	0.395 E−01	0.561 E−02
POT	0.442 E−01	0.608 E−02

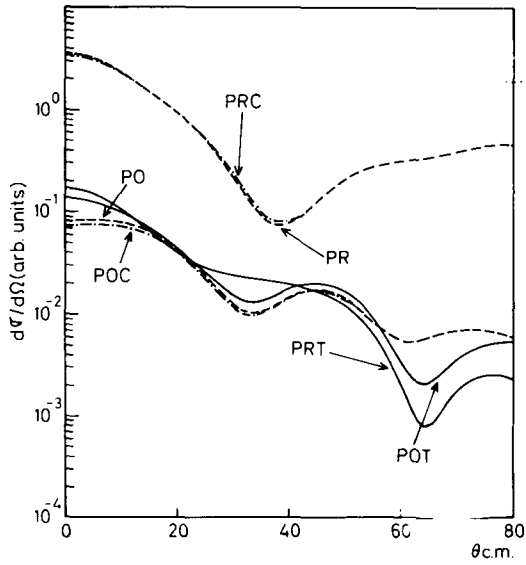

Form	$V_{cor-clu}$	$V_{cor-clu}*V_{coul}$	$V_{cor-clu}*V_{coul}*V_{bA}-U$
Prior	PR	PRC	PRT
Post	PO	POC	POT

Fig. 11. Effect of interaction terms in DWBA calculations for $^{14}N(^{6}Li, d)^{18}F$ (2^+ at 2.524 MeV). All calculations have normalization factor 1.

6.2. FORM FACTORS

The BDV cluster model formalism has been used in the calculation for the unbound Gamow wave functions to describe the states populated in ^{18}F. An alternative parametrization of the cluster core potential suggested by Buck and Pilt [8]) (cosh type in table 4) has been used throughout. Radius and diffuseness parameters have been taken from this reference. The depths of the potentials were adjusted to fit the "binding" energy of each state in the numerical calculation and are shown in table 4 where also the single-particle widths extracted from the complex part of the energy eigenvalue of the bound states are shown.

The Gamow wave functions obtained were input for the DWBA calculation of the transition amplitudes. The square of the absolute values for the real and imaginary parts for some Gamow state wave functions are plotted in fig. 12. For comparison, the bound-state solutions obtained with the DWBA code for the same parameterized cluster-core potential and using a fictitious binding energy of -0.1 MeV are also displayed. They show different asymptotic behaviours since for the

TABLE 4

States in ^{18}F

E_x (MeV)	J^π	L N	$2N+L$	V_{depth} $(-V_0)$ (MeV)	$\Gamma^2_{s.p.}$(MeV) (calc.)	Γ (MeV)[a]) (exp.)	Pot. type
5.3	4^+	4 2	8	175.5	0.372 E−07	0.212 E−07	cosh
		4 2	8	170.5	0.580 E−03		cosh
6.5	5^+					0.800 E−03	
		6 1	8	188.8	0.636 E−06		cosh
9.58	6^+	6 1	8	178.7	0.527 E−02	0.550 E−01	cosh
		6 1	8	172.6	0.503 E−01		cosh
11.2	(7^+)						
		8 0	8	196.8	0.707 E−04		cosh
14.1	8^+	8 0	8	188.9	0.321 E−02		cosh

The potential for the α-cluster is given by

$$V(r) = V_0 f(r) + V_c(r),$$

with

$$f(r) = \frac{1+\cosh(R/a)}{\cosh(r/a)+\cosh(R/a)} \qquad \text{(cosh type)},$$

$$a = 0.8 \text{ fm}, \qquad r_0 = 0.555 \text{ fm},$$

and $V_c(r)$ the potential due to a charged sphere of radius R_c

for

$$r_{0c} = 0.764 \text{ fm}$$

$$R = r_0(A_\alpha^{1/3} + A_{^{14}N}^{1/3}) = 2.25 \text{ fm}$$

$$R_c = r_{0c}(A_\alpha^{1/3} + A_{^{14}N}^{1/3}) = 3.1 \text{ fm}$$

[a]) From ref. [39]).

unbound description the probability of finding the α-cluster at larger radii will be higher than for the bound model.

The potential obtained by Kubo and Hirata [21]) was chosen for the lighter system (α-d) potential. They postulated a very simple form of the $V_{\alpha d}$ interaction which gives a very good agreement in the shape of the potential as well as in the wave function, with the predictions of Hasegawa and Nagata [27]) for the two clusters in the ^{6}Li ground state, with exchange effects exactly treated. Kubo and Hirata assume a Saxon-Woods shape for the effective interaction, with radius parameter $R = 1.0$ fm and diffuseness $a = 0.65$ fm. With these parameters and the requirements of one node and $L = 0$ for the relative motion of the clusters, the potential depth was adjusted by the program in order to give a separation energy of 1.473 MeV.

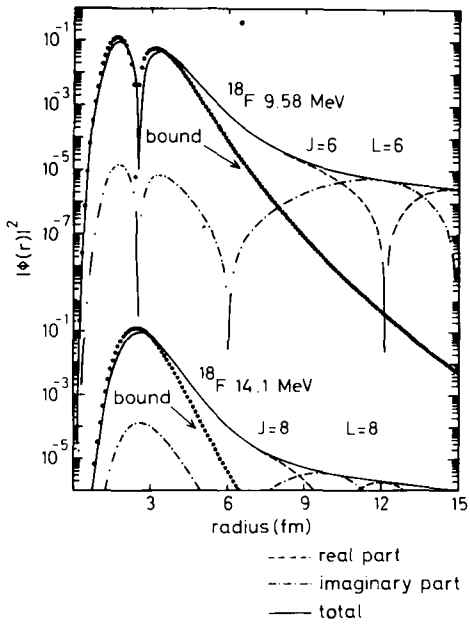

Fig. 12. Gamow-state wave functions for the 9.58 MeV and 14.1 MeV unbound states in ^{18}F. The slightly bound wave functions (−0.1 MeV binding energy) are also plotted.

6.3. SPECTROSCOPIC FACTORS

For a direct four-nucleon transfer where a cluster with $T = 0$ is considered, the description of its internal structure as an α-particle is the most likely one. In the ^{14}N(^{6}Li, d)^{18}F reaction, where states of a 4p–2h rotational band are strongly populated, the cluster picture gives a total quantum number $Q = 2N + L = 8 = (\mathrm{sd})^4$. The wave function which describes the four particles of the cluster in ^{18}F, carries an SU(3)(λ, μ) label (8, 0) for $L = 8, 6, 4, 2, 0$. As a predominantely 4p–2h description is expected for the resultant ^{18}F states dominated by an $(\mathrm{sd})^4$ configuration, shell-model calculations were performed for a ^{12}C core plus six particles in the $0p_{\frac{1}{2}}$, $0d_{\frac{5}{2}}$ and $1s_{\frac{1}{2}}$ orbits with a Reehal and Wildenthal two-body interaction [28]). The members of the $K^\pi = 1^+$ band strongly populated were searched. The resultant energies, percentages of 4p–2h and 2p–0h configurations for the different spins are shown in table 5. The energies of several experimental states are very well matched, although the basis used is obviously largely truncated. The overlaps between these shell-model states and the $(\mathrm{sd})^4$ cluster states were calculated and their values are also shown in table 5. It can be seen that the largest amplitudes are the ones predicted for the states strongly populated in the reaction, and these were therefore used as theoretical spectroscopic factors.

TABLE 5

Four nucleon parentage amplitudes for $(\lambda, \mu) = (8, 0)$ transfer on ^{14}N

^{18}F states	E_x(MeV) (theor.)	E_x(MeV) (exp.)	% of 4p–2h	% of 2p–0h	L	REWIL inter. overlap
					0	−0.078
1_1^+	0.0	0.0	31.2	64.4		
					2	0.0002
					0	−0.528
1_2^+	1.879	1.7	95.0	0.20		
					2	0.041
2_1^+	3.03	2.52	64.1	27.6	2	0.455
2_2^+	3.65	3.06	73.1	24.6	2	0.651
					2	−0.023
3_1^+	0.314	0.937	27.0	69.4		
					4	−0.036
					2	0.651
3_2^+	3.12	3.35	94.9	1.40		
					4	−0.018
					2	0.166
3_3^+	4.07	4.119	47.5	31.0		
					4	0.257
4_1^+	5.56	4.65	46.8		4	−0.340
4_2^+	6.07	5.298	78.5		4	0.726
					4	−0.010
5_1^+	0.77	1.12	29.0	67.1		
					6	0.072
					4	−0.826
5_2^+	5.69	6.56	96.1	0.60		
					6	−0.014
6_1^+	8.54		35.6		6	−0.009
6_2^+	9.71	9.58	89.8		6	−0.844
					6	0.912
7_1^+	9.22	(11.22)	96.3			
					8	0.031
8_1^+	13.84	14.18	93.6		8	0.967

A similar analysis was performed for the lighter system, $^6Li_{g.s.} = \alpha$-d, and values for the contribution of different relative L-values were obtained. They showed 91.78 % of $L = 0$, 0.58 % of $L = 1$ and 7.64 % of $L = 2$, with values for the overlaps of 0.958, 0.076 and −0.276, respectively.

6.4. COMPARISON OF THE DWBA PREDICTIONS WITH THE EXPERIMENT

The experimental cross sections obtained in $^{14}N(^6Li, d)^{18}F$ and the normalisations of the DWBA predictions to the experimental cross sections are shown in figs. 3a and 3b. The normalisation coefficients and the theoretical

TABLE 6

Normalisation factors and spectroscopic factors for the $^{14}N(^6Li, d)^{18}F$ reaction

E_x (MeV)	J^π	N	L	$2N+L$	$\mathcal{N}$	S_{DWBA}	S_{theor}	S_{rel}
5.3	4^+	2	4	8	0.164	0.159	0.152	0.147
		2	4	8	0.272	0.263	0.196	0.190
6.5	5^+							
		1	6	8			0.54 E−4	
9.58	6^+	1	6	8	0.190	01.84	0.204	0.198
		1	6	8	0.172	0.167	0.232	0.225
11.2	(7^+)							
		0	8	8			0.28 E−3	
14.1	8^+	0	8	8	0.268	0.260	0.268	0.260

$\mathcal{N}$ is the ratio of the experimental cross sections to the DWBA calculations $S_{DWBA} = \mathcal{N}/C_p^2 S_p C_R^2$, where S_p is the calculated spectroscopic factor for ^6Li = 1.032 and C_p and C_R are the isospin Clebsch-Gordan coefficients for the projectile and residual nucleus respectively. S_{rel} = relative theoretical spectroscopic factor normalised to the 8^+ state.

spectroscopic factors are shown in table 6. Fairly good agreement in shape and magnitude is observed for the five states. Even the attempted 7^+ calculation for the 11.2 MeV state seems to reproduce the experimental shape. Very good agreement between experimental and relative spectroscopic factors is found for the 4^+ at 5.3 MeV and the identified (in sect. 5) 6^+ and 8^+ states (9.58 MeV and 14.1 MeV). Fairly good agreement is found for the 6.5 and 11.2 MeV states which show normalisation values that differ in approximately 35 % from the relative spectroscopic factors. For the odd-spin states, two L-contributions have to be considered, $L = J-1$ and $J+1$. Thus, the 5^+ and 7^+ cross sections will arise from an incoherent sum of $L = 4$, 6 and $L = 6$, 8 DWBA calculations, respectively. For these cases, the theoretical parentage amplitude estimations showed a particularly large strength for the low L-values and as far as agreement in shape and normalisation, our data seem to confirm the predictions.

The relative agreement found between spectroscopic strengths for the analysed states, is consistent with identifying them as members of the same rotational band. Despite the small discrepancies found in the comparison of the spectroscopic factors for the odd-spin states, it is believed that they are not inconsistent with a direct α-transfer mechanism and with their identification as members of the 1^+ band.

Considering the light system, the angular momentum coupling for the ^6Li projectile allows L-values 0, 1 and 2; only the $L = 0$ state will have some importance as shown in the previous section, and no appreciable contribution to incoherent addition of cross sections will be introduced by the projectile system.

Important multistep contributions to the reaction mechanism involved in the

(^{6}Li, d) reaction on ^{12}C have been suggested by different authors [29,30]) based on that neither a direct DWBA α-transfer nor a Hauser-Feshbach calculation can fully explain the observed angular distribution data. In the present analysis the data seem to be well described by DWBA calculations and also the extracted spectroscopic factors show to be in agreement with those predicted from shell-model calculations.

7. Conclusions

Experimental evidence for the existence of the $K^\pi = 1^+$ band in ^{18}F is found in the literature. Rolfs *et al.* [7]) carried out the identification of the first five members of such band (1^+ (1.701 MeV), 2^+ (2.532 MeV), 3^+ (3.358 MeV), 4^+ (5.298 MeV), 5^+ (6.567 MeV)) and predicted the location of the next member $J^\pi = 6^+$ at approximately 9.2 MeV. Out of their experimental measurements, Cobern *et al.* [1]) suggested that the 9.58 and 11.2 MeV states could be regarded as candidates for the 6^+ and 7^+ members of the band. The results of the angular correlation χ^2 tests performed in this work gave definite parity and spin assignments to two of the high-lying states (6^+ (9.58 MeV) and 8^+ (14.1 MeV)) while due to the structureless correlation of the 11.2 MeV state its parity and spin remain undetermined. An energy scheme from 1^+ to 8^+ can be drawn (fig. 13) assuming the 11.2 MeV state to be a member of the $K^\pi = 1^+$ band. A good agreement between the measured excitation energies and the pattern expected for the highest members of this band is shown here.

From the comparison between the DWBA calculations and the experimental data, the states strongly populated in the four nucleon transfer reaction on ^{14}N may be seen as resulting from a direct α-transfer mechanism. Prior and post agreement was obtained. The even-spin states angular distributions were shown to be in accordance with theoretical predictions in both magnitude and shape, and as a result of the analysis of relative spectroscopic factors should be regarded as

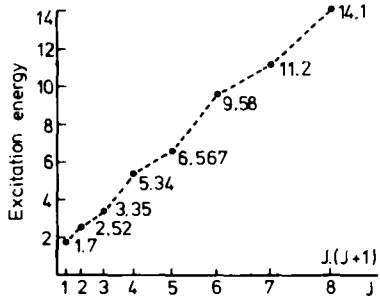

Fig. 13. Energy scheme of the $K^\pi = 1^+$ rotational band in ^{18}F.

members of the same rotational band. The DWBA study for the 9.58 and 14.1 MeV states complements the spin assignments performed with the angular correlation analyses. The cross sections for the odd-spin states seem to be fairly well described by DWBA calculations as far as shape is concern, and despite some small discrepancies in the spectroscopic factors, the direct transfer analysis seems to be successful. Despite the fact that no spin assignment has been made for the 11.2 MeV state, the data are consistent with a $J^\pi = 7^+$ assignment. It can be concluded that a fairly good description of the structure of the analysed states, as well as the reaction mechanism involved has been completed.

The authors are grateful to Dr. K. Snover for helpful discussions and comments.

Appendix A

RADIOACTIVE DECAY OF A NUCLEUS

Direct reactions as knock-on, stripping or inelastic scattering can lead to orientation effects in the residual nucleus [31]. When these polarization effects take place, a correlation between the direction of the outgoing ejectile and the direction of the emission of any radiation or particle subsequently emitted by the residual nucleus can be observed. We shall consider here a sequential process in which after a direct transfer reaction, the emission of a particle from the recoil nucleus occurs. The whole process is summarized in fig. 14 where i, m_i, I, m_I, I', $m_{I'}$, i', $m_{i'}$, I'', $m_{I''}$, i'', $m_{i''}$ identify the spins and their z-projections for the incident particle, target nucleus, recoil nucleus, ejectile, residual nucleus, and decay particle, respectively. The scattering angle θ_1 is measured in the total centre-of-mass frame whereas the disintegration angle is measured in the recoil nucleus centre-of-mass frame, and they are both defined relative to the beam direction. T_r and T_d identify the transition amplitudes for the transfer and decay processes respectively ($T_r(m_i m_I, m_{i'} m_{I'}; \Omega_1)$ and $T_d(m_{I'}, m_{i''} m_{I''}; \Omega_2)$). The probability of having the decay particle

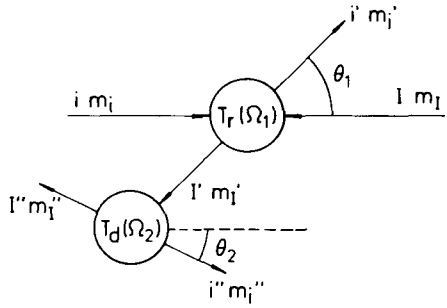

Fig. 14. Scheme of a transfer and decay process.

emerging in the Ω_2 direction after the ejectile has been emitted in the Ω_1 direction will be given by the correlation function $W(\Omega_1, \Omega_2)$:

$$W(\Omega_1, \Omega_2) = \sum_{\substack{m_i m_I \\ m_{i'} m_{I'} \\ m_{i'}}} \left| \sum_{m_{I'}} T_r(m_i m_I, m_{i'} m_{I'}; \Omega_1) T_d(m_{I'}, m_{i'} m_{I''}; \Omega_2) \right|^2, \tag{A.1}$$

assuming that the ejectile has no influence on the recoil nucleus disintegration process. When studying reactions in which the involved colliding nuclei or their products have intrinsic spins, it is often inconvenient to treat the process in terms of the z-projections of the spins, since these values depend on the choice of the z-direction. Clearly, the dynamics of the collision can not depend on the choice of the coordinate system. It is useful in general to work in the so-called channel-spin representation for both, the transfer and decay processes. The system before the collision will be defined by the type of incoming particles, the channel spin s (the total spin in the incident channel, formed by vector addition of the spin of the projectile and the spin of the target), and the relative orbital angular momentum l. The spin s and the momentum l add together to give the total angular momentum J of the system. This total J must be preserved in the collision process and as a result of this, the exit channel spin s' (formed by vector addition of spins of the ejectile and recoil nucleus) added to the relative orbital momentum l', give the same total J. For the decay process, the channel spin s'' (formed by vector addition of the spins of the decay particle and the residual nucleus) and the relative orbital momentum l'' combine to give the spin of the recoil nucleus (I'). When the phenomenological description of the reaction process is done in the scattering matrix formalism, only the asymptotic wave functions for the entrance and exit channels are treated explicitly. The relation between these incoming and outgoing waves gives the scattering matrix which contains all the physical information about the process. The asymptotic form of the reaction wave function in the exit channel can be given equivalently in terms of the scattering matrix as well as in terms of the reaction amplitudes, and the relation between these two is given by [32])

$$T_r(m_i m_I, m_{i'} m_{I'}; \Omega_1) = \sum_{\substack{ss'J \\ m_s m_{s'} \\ m_J}} \sum_{\substack{ll' \\ m_{l'}}} (2l+1)^{\frac{1}{2}} (Iim_I m_i | s\, m_s)(ls\,0\, m_s | J\, m_J)$$

$$\times (l's' m_{l'} m_{s'} | J m_J)(I'i' m_{I'} m_{i'} | s' m_{s'})$$

$$\times S^J_{s'l'sl}\, Y_l^{m_l}(\Omega_1), \tag{A.2}$$

where $S^J_{s'l'sl}$ is given by the mechanism of the reaction. In a similar way Da Silveira [19]) treats the decay process in the channel spin representation, expressing

the decay amplitude in terms of the disintegration matrix elements $S^{I'}_{s''l''}$:

$$T_d(m_I m_{i''} m_{I''};\ \Omega_2) = \sum_{\substack{s'' \\ m_{s''}}} \sum_{\substack{l'' \\ m_{l''}}} (I''i''m_{I''}m_{i''}|s''m_{s''})(s''l''m_{s''}m_{l''}|I'm_{I'}) \times S^{I'}_{s''l''} Y^{m_{l''}}_{l''}(\Omega_2). \tag{A.3}$$

A very general expression for the correlation function is obtained replacing the transition amplitudes given above into eq. (A.2). For computational reasons, since "reduced amplitudes" ($\beta^l_{m_l}$) were obtained from DWBA codes, the transition amplitude for the reaction process was replaced by the form [24]):

$$T_r(\theta) = \sum_{lsj} (2l+1)^{\frac{1}{2}} A_{lsj} (-)^{i'-m_{i'}} (Ijm_I m_j|I'm_{I'})(lsm_l m_s|jm_j) \times (ii'm_i(-m_{i'})|sm_s)\beta^l_{m_l}(\theta), \tag{A.4}$$

for a stripping reaction given by A(a, b)B. Where a particle x is transferred from a = b+x (x bound to the core b with angular momentum l_1) to the core A = B−x (with angular momentum l_2), satisfying the sum rules

$$\boldsymbol{j} = \boldsymbol{I} - \boldsymbol{I}', \qquad \boldsymbol{l} = \boldsymbol{l}_1 - \boldsymbol{l}_2,$$
$$\boldsymbol{s} = \boldsymbol{i} - \boldsymbol{i}', \qquad \boldsymbol{j} = \boldsymbol{l} + \boldsymbol{s}. \tag{A.5}$$

A_{lsj} is the spectroscopic coefficient defined by [33])

$$A_{lsj} = i^l (2l+1)^{\frac{1}{2}} (2i+1)^{\frac{1}{2}} J\gamma_1\gamma_2 W(j_1, l_1, j_2, l_2;\ s_x, l)\delta(s, j_1)\delta(j, j_2).$$

Here J is the jacobian of the coordinate transformation, γ_1 and γ_2 the real spectroscopic amplitudes for the cluster x in nuclei a and B, respectively, s_x the spin of the transferred cluster, $j_1 = l_1 + s_x$ and $j_2 = l_2 + s_x$, and W the Racah coefficient for the specified quantities. The $W(\Omega_1, \Omega_2)$ function results then in the following expression:

$$W(\Omega_1, \Omega_2) = N \sum_{\substack{m_i m_j \\ m_{i'} \\ m_{I'}}} \left| \sum_{m_{I'}} \left\{ \sum_{lsj} A_{lsj} (-1)^{i'-m_{i'}} (Ijm_I m_j|I'm_{I'}) \times (lsm_l m_s|jm_j)(ii'm_i(-m_{i'})|sm_s)\beta^l_{m_l}(\theta_1) \times (I''i''m_{I''}m_{i''}|s''m_{s''})(s''l''m_{s''}m_{l''}|I'm_{I'}) S^{I'}_{s''l''} Y^{m_{l''}}_{l''}(\theta_2) \right\} \right|^2 .$$

All the different l'' contributions to the angular correlation function have to be included through the decay matrix $S^{I'}_{s''l''}$. When the emission of an α-particle takes

place ($i'' = 0$, $m_{i''} = 0$ and s'' unique), some particular case can be derived if l'' is unique. The decay mechanism (contained in the S-matrix) will not affect the shape of the angular correlation, acting only as part of the normalisation coefficient.

Appendix B

THE $S^{I'}_{s''l''}$ DECAY MATRIX

As seen in appendix A, for evaluating the theoretical expression for the angular correlation when more than one l'' value intervenes, the matrix elements $s^{I'}_{s''l''}$ have to be given as input data. It is important then to give a model from which their values could be obtained or at least their range of variation could be estimated. For all α-decay analyses performed in this work, the cluster model picture has been followed, and according to that, at most two l'' values will contribute to the theoretical expression for the angular correlation, as it is the case for certain total angular momentum values in ^{18}F leading to the ground state (1^+) of the daughter nucleus (^{14}N).

The angular correlation defined in appendix A is the probability that the α-particle should emerge in direction Ω_2 after the ejectile (deuteron) has come out in direction Ω_1. By integration of such quantity over all Ω_1 and Ω_2 values one obtains the product of the total cross section for the formation of the state in ^{18}F times the probability for that state to decay by α-emission, given by the ratio between the α-decay width over the total width of the state:

$$\int W(\Omega_1, \Omega_2)\mathrm{d}\Omega_1\mathrm{d}\Omega_2 = C\sigma_1(\text{formation})\Gamma^\alpha/\Gamma_{\text{tot}}. \tag{B.1}$$

Replacing $W(\Omega_1, \Omega_2)$ by the most general form given in eq. (A.7), and making use of the orthogonality properties of spherical harmonics and Clebsch-Gordan coefficients, the integral can be expressed in a very simple form:

$$\sum_{l''} |S^{I'}_{s''l''}|^2 \, \sigma_1(\text{formation}) = C\sigma_1(\text{formation})\Gamma^\alpha/\Gamma_{\text{tot}}, \tag{B.2a}$$

$$\sum_{l''} |S^{I'}_{s''l''}|^2 = C\Gamma^\alpha/\Gamma_{\text{tot}} = C\sum_{l''} \Gamma^\alpha_{l''}/\Gamma_{\text{tot}}, \tag{B.2b}$$

where all the real and positive normalisation constants have been grouped in C. When two l'' values are considered, the $S^{I'}_{s''l''}$ matrix must satisfy

$$\sum_{l''} \left| \frac{S^{I'}_{s''l''}}{(C\Gamma^\alpha/\Gamma_{\text{tot}})^{\frac{1}{2}}} \right|^2 = 1. \tag{B.3}$$

As $C\Gamma^\alpha/\Gamma_{\text{tot}}$ is a real factor common to all l'' contributions, it will not affect the

structure of the angular correlation function, acting only as a normalisation constant. It will be possible then to estimate how different complex $S^{I'}_{s'l'}$ values, which comply with the requirement

$$|S^{I'}_{s'l_1}|^2 + |S^{I'}_{s'l_2}|^2 = 1, \qquad \text{(B.4)}$$

influence the final angular correlation shape. In this work, when two orbital angular momenta l'' are required for a theoretical calculation, different values of $S^{I'}_{s'l''}$ have been used in the range given by eq. (B.4) and with phases given by $\phi = 0$, $\frac{1}{2}\pi$, π and $\frac{3}{2}\pi$. The theoretical angular correlations have been compared to the experimental data with χ^2 tests, and the values for the best fit used in the final chi-square comparison.

References

1) M. E. Cobern and P. D. Parker, Phys. Rev. **C15** (1977) 1929
2) R. Middleton, L. M. Polsky, C. H. Holbrow and K. Bethge, Phys. Rev. Lett. **21** (1968) 142
3) A. Cunsolo, A. Foti, G. Imme, G. Pappalardo and G. Raciti, Phys. Rev. **C24** (1981) 476
4) K. Meier-Ewert, K. Bethge and K. O. Pfeiffer, Nucl. Phys. **A110** (1968) 142
5) B. Buck, C. B. Dover and J. P. Vary, Phys. Rev. **C11** (1975) 1803
6) H. S. Bradlow, W. D. M. Rae, P. S. Fisher, N. S. Godwin, G. Proudfoot and D. Sinclair, Nucl. Phys. **A314** (1978) 207
7) C. Rolfs, H. P. Trautvetter, R. E. Azuma and A. E. Litherland, Nucl. Phys. **A199** (1973) 289
8) B. Buck and A. A. Pilt, Nucl. Phys. **A280** (1977) 133
9) K. P. Artemov, V. Z. Goldberg, I. P. Petrov, V. P. Rudakov, I. N. Serikov and V. A. Timofeev, Phys. Lett. **37B** (1971) 61
10) A. D. Panagiotou, J. C. Cornell, N. Anyas-Weiss, P. N. Hudson, A. Menchaca- Rocha, D. K. Scott and B. E. F. Macefield, J. of Phys. **7** (1974) 1748
11) M. Avril, M. Lepareux, N. Saunier, A. Foti, G. Pappalardo and A. Strazzeri, J. de Phys. **36** (1975) 229
12) K. P. Artemov, V. Z. Goldberg, I. P. Petrov, V. P. Rudakov, V. A. Timofeev, R. Wolski and J. Szminder, Sov. J. Nucl. Phys. **22** (1976) 125
13) J. M. Lambert, P. A. Treado, D. Haddad, R. A. Moyle and J. C. Sessler, Phys. Rev. Lett. **27** (1971) 820
14) H. S. Bradlow, W. D. M. Rae, P. S. Fisher, N. S. Godwin, G. Proudfoot and D. Sinclair, Nucl. Phys. **A314** (1978) 171
15) L. J. House and K. W. Kemper, Phys. Rev. **C17** (1978) 79
16) R. G. Stokstad, Wright Nuclear Structure Research Lab. Internal Report no. 52, Yale Univ. (1972) unpublished
17) K. M. Abdo, L. C. Dennis, A. D. Frawley and K. W. Kemper, Nucl. Phys. **A377** (1982) 281
18) L. C. Dennis, A. Roy, A. D. Frawley and K. W. Kemper, Nucl. Phys. **A359** (1981) 455
19) E. F. Da Silveira, Contrib. to XIV Winter Meeting on nuclear physics, Bormio (1976)
20) R. M. DeVries, Phys. Rev. **C11** (1975) 2105
21) K. I. Kubo and M. Hirata, Nucl. Phys. **A187** (1972) 186
22) R. M. DeVries, computer code LOLA (unpublished)
23) W. D. M. Rae and N. S. Godwin, DWAVF Oxford code (unpublished)
24) T. Tamura and K. S. Low, Comp. Phys. Comm. **8** (1974) 349
25) C. M. Perey and F. G. Perey, Atom. Nucl. Data Tables, **17** (1976) 1
26) W. Fitz, R. Jahr and R. Santo, Nucl. Phys. **A101** (1967) 449
27) H. Hasegawa and S. Nagata, Prog. Theor. Phys. **38** (1967) 1188
28) B. S. Reehal and B. H. Wildenthal, Part. and Nuclei, **6** (1973) 137

29) C. W. Glover and K. W. Kemper, Nucl. Phys. **A366** (1981) 469
30) A. Consoli, A. Foti, G. Pappalardo, G. Raciti and N. Saunier, Phys. Rev. **C18** (1978) 856
31) W. Tobocman, Theory of direct nuclear reactions (Oxford University Press, 1961)
32) J. M. Blatt and L. C. Biedenharn, Rev. Mod. Phys. **24** (1952) 258
33) T. Kamimuri and H. Yoshida, Nucl. Phys. **A129** (1969) 265
34) H. F. Lutz, J. B. Mason and M. D. Karvelis, Nucl. Phys. **47** (1963) 521
35) R. DeSwiniarski, A. Genoux-Lubain, G. Bagieu, J. F. Cavaignac, D. H. Worledge and J. Raynal, Phys. Lett. **43B** (1973) 27
36) D. Denhard and H. M. Hintz, Phys. Rev. **C1** (1970) 460
37) I. F. Hansen, M. L. Stelts, J. G. Vidal, J. J. Wesolowski and V. A. Madsen, Phys. Rev. **174** (1968) 1155
38) R. H. Davis, Proc. Third Conf. on reactions between complex nuclei, University of California Press (1963) p. 61
39) F. Ajzenberg-Selove, Nucl. Phys. **A300** (1978) 1